Applied Thermal Engineering 213 (2022) 118703

Contents lists available at ScienceDirect

Applied Thermal Engineering

journal homepage: www.elsevier.com/locate/ate

Research paper

Influence of pressure recovery on the performance of an induced draught air-cooled condenser under windless and windy conditions

G.M. Bekker *, C.J. Meyer, S.J. van der Spuy

Department of Mechanical and Mechatronic Engineering, Stellenbosch University, Private Bag X1, Matieland 7602, South Africa

ARTICLE INFO

Keywords:
Air-cooled condenser
Induced draft
Pressure recovery
Conical diffuser
Wind effects

ABSTRACT

This research aims to enhance the performance of a 20-fan induced draught air-cooled condenser (ACC) by increasing the airflow rate and heat rejection rate of the ACC. These improvements are achieved through pressure recovery, which is the conversion of the dynamic pressure loss at the fan outlets into static pressure. Two different conical diffusers are attached to the outlets of the ACC's fans to facilitate pressure recovery. The shorter diffuser has a length equal to 20% of the fan diameter and an included angle of $2\theta = 40°$; the longer diffuser is 40% the length of the fan diameter with $2\theta = 32°$. The performance of this five-by-four ACC is analysed with and without these diffusers through numerical simulation in OpenFOAM. The analysis is performed under windless and windy conditions. The added diffusers increase the volumetric and thermal effectiveness of the ACC by 2.5% and 2.0%, respectively, under windless conditions. At wind speeds of 3, 6 and 9 m/s, the gain in volumetric effectiveness declines to 1–2%, while the gain in thermal effectiveness varies in the range of 0–5%. The longer of the two diffusers yields greater improvements, especially at higher wind speeds.

1. Introduction

In induced draught air-cooled condensers (ACCs), axial flow fans draw air through upstream heat exchangers to condense the process fluid flowing inside the heat exchanger tubes. The dynamic pressure at the fan outlets is a loss to the fan system. This study aims to reduce that dynamic pressure loss in order to increase the effective fan static pressure rise of the ACC's fans. This conversion of dynamic pressure into static pressure is termed pressure recovery. As the effective pressure rise of the fans increases, the operating air volume flow rate through the ACC increases, which allows for improved heat transfer capability.

Downstream stator blade rows and diffusers are capable of pressure recovery [1,2]. Walter et al. [3] theoretically illustrated that the use of a downstream stator blade row could increase the static efficiency of a typical axial flow fan by 7%. Adding an annular diffuser to that fan-stator combination could increase the fan static efficiency by a further 20%.

Bekker et al. [4] numerically investigated stator blade rows, conical and annular diffusers, and combinations of these for an axial flow fan. They designed discharge diffusers for the M-fan of Wilkinson et al. [5] through parametric studies. By attaching a particular annular diffuser to the fan outlet, they reported a 6.3% increase in operating volume flow rate and a 20% increase in fan static efficiency. The length of this diffuser was equal to the fan diameter, and the inner and outer diffuser walls were angled at 22° from the axial direction.

Bekker et al. [6] considered the length and wide wall angles of the aforementioned diffuser impractical for ACC application. They therefore repeated the parametric studies for shorter diffuser lengths. It was found that a conical diffuser of length equal to 20% of the fan diameter, or $l_{dif} = 0.2d_F$, with an included angle of $2\theta = 40°$ produced promising pressure recovery coefficients over a range of airflow rates. Another conical diffuser with $l_{dif} = 0.4d_F$ and $2\theta = 32°$ also produced promising pressure recovery results. Bekker et al. [6] then obtained the performance characteristics of these fan-diffuser combinations using an ISO 5801 [7] fan test setup of type A (i.e. a free-inlet-free-outlet setup). At the design flow rate of the M-fan, they found that the $l_{dif} = 0.2d_F$ diffuser increased the fan static pressure rise by 17.6% (relative) and the fan static efficiency by 8.9% (absolute). With the $l_{dif} = 0.4d_F$ diffuser, 21.9% and 11.7% increases were reported, respectively.

Although it is well documented that conical diffusers can enhance fan performance in induced draught ACCs [1,8], there is a void in the literature regarding the extent of these performance improvements. Bekker et al. [6] also pointed out that diffuser design charts are often inappropriately used in combination with axial flow fans to predict fan-diffuser performance. The current study aims to quantify the improvements in induced draught ACC performance by comparing the

* Corresponding author.
E-mail addresses: gerhard@spatialedge.co.za (G.M. Bekker), cjmeyer@sun.ac.za (C.J. Meyer), sjvdspuy@sun.ac.za (S.J. van der Spuy).

https://doi.org/10.1016/j.applthermaleng.2022.118703
Received 21 October 2021; Received in revised form 17 March 2022; Accepted 18 May 2022
Available online 26 May 2022

Nomenclature

A	Area, m^2
c	Chord length, m
C_D	Drag coefficient
C_L	Lift coefficient
c_p	Specific heat at constant pressure, J/(kg K)
C_μ, β^*	Turbulence model constants, 0.09
d_F	Fan diameter, m
e	Specific internal energy, J/kg
F	Force, N
g	Gravitational acceleration, m/s^2
h	Heat transfer coefficient, $W/(m^2 K)$
H_F	Fan height, m
k	Turbulence kinetic energy, m^2/s^2; or thermal conductivity, W/(m K)
k_D	Darcy coefficient, m^{-2}
k_F	Forchheimer coefficient, m^{-1}
K_{he}	Isothermal pressure loss coefficient
L	Length, m
l_{dif}	Diffuser length, m
$\dot{m}$	Mass flow rate, kg/s
n	Normal direction
n_{Fb}	Number of fan blades
Ny	Characteristic heat transfer parameter, m^{-1}
p	Pressure, Pa
P_F	Fan shaft power consumption, W
Pr	Prandtl number
$\dot{Q}$	Heat transfer rate, W
R	Gas constant, J/(kg K)
r	Radius, m
Ry	Characteristic flow parameter, m^{-1}
T	Temperature, °C
t	Actuator disc thickness, m
U	Overall heat transfer coefficient, $W/(m^2 K)$
u	Velocity, m/s
u_*	Friction velocity, m/s
V	Volume, m^3
$\dot{V}$	Volume flow rate, m^3/s
W	Width, m
x, y, z	Cartesian coordinate directions
y	Wall-normal distance, m
y^+	Sublayer-scaled wall-normal distance
z	Height from ground level, m
z_0	Surface roughness height, m
α_{att}	Angle of attack, deg
β	Relative flow angle, deg
β_1	Turbulence model constant, 0.075
γ	Blade setting angle, deg
ϵ	Heat exchanger effectiveness
2θ	Diffuser included angle, deg
κ	Von Kármán constant, 0.41
μ	Dynamic viscosity, kg/(m s)
ν	Kinematic viscosity, m^2/s
ρ	Density, kg/m^3
σ	Blade solidity ratio
2ϕ	V-frame apex angle, deg
ω	Specific turbulence dissipation rate, s^{-1}

Subscripts

a	Air
atm	Atmospheric
b	Bundle
fr	Frontal
he	Heat exchanger
i	Inlet
id	Ideal
L, D	Lift and drag components
m	Mean
o	Outlet
R	Relative
ref	Reference
s	Steam
tot	Total
u	Fan unit
x, θ	Axial and tangential components

volumetric and thermal effectiveness of an ACC without diffusers to that of the same ACC with discharge conical diffusers. Additionally, this study aims to illustrate how wind affects the performance of such an ACC with and without discharge diffusers.

The $l_{dif} = 0.2d_F$ with $2\theta = 40°$ and $l_{dif} = 0.4d_F$ with $2\theta = 32°$ conical diffusers of Bekker et al. [6] were adopted for the current study to enhance the performance of a five-by-four induced draught ACC. The fan units in the ACC employed Wilkinson et al.'s [5] M-fan to draw air through the heat exchangers oriented in a V-frame configuration. The effectiveness of this 20-fan ACC was evaluated under wind-still and windy operating conditions.

2. Numerical modelling

The open-source computational fluid dynamics code, OpenFOAM-v1906, was used to solve the Reynolds-averaged Navier–Stokes (RANS) equations. This section documents the numerical models and solution strategies that were used to simulate an induced draught ACC.

2.1. Numerical solvers and settings

Computations were performed using a steady-state solver based on the `rhoPorousSimpleFoam` solver. It is a density-based compressible solver for turbulent flows. Louw et al. [9] incorporated an axial flow fan model into the momentum equation and a heat transfer model into the energy equation of this solver. The solver also allows for the incorporation of porous media, which was used to account for the pressure drop due to the heat exchangers. Furthermore, through OpenFOAM's finite volume options, the buoyancy force, $\rho\mathbf{g}$, and buoyancy energy, $\rho(\mathbf{g} \cdot \mathbf{u})$, were added to the momentum and energy equations, respectively.

Bekker et al. [4] found that the standard k-ω turbulence model [10] predicted the flow inside a conical diffuser with swirling flow reasonably accurately. Bekker et al. [6] also found that the k-ω model performed well with the actuator disc model, which is the axial flow fan model used in the current study. Therefore, the k-ω turbulence model was selected to close the RANS equations.

Gauss' theorem was employed for the discretisation of gradient terms. Cell gradients were limited by bounding face values by the minimum and maximum values of neighbouring cells. The divergence of velocity and internal energy was discretised using a bounded linear-upwind scheme of second-order accuracy. The divergence of turbulence

Table 1
Iterative solver settings.

Governing variable	Solver	Smoother or preconditioner	Tolerance	Relative tolerance	Under-relaxation
p	GAMG[a]	DICGaussSeidel[b]	10^{-6}	10^{-3}	0.2
u	PBiCGStab[c]	DILU[d]	10^{-8}	0	0.5
e	PBiCGStab	DILU	10^{-8}	10^{-3}	0.3
k, ω	PBiCGStab	DILU	10^{-8}	10^{-3}	0.6

[a]Geometric agglomerated algebraic multigrid solver.
[b]Simplified diagonal-based incomplete Cholesky smoother with Gauss–Seidel post-smoothing.
[c]Preconditioned bi-conjugate gradient stabilised solver.
[d]Simplified diagonal-based incomplete LU preconditioner.

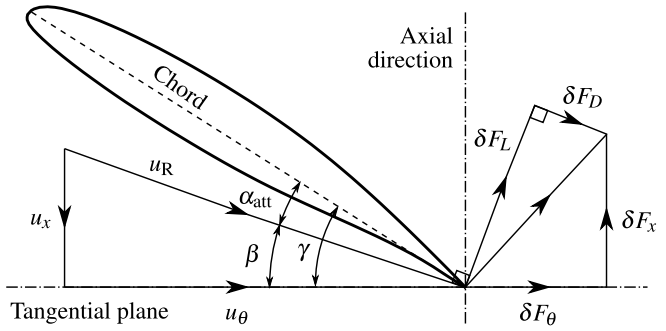

Fig. 1. Forces on blade element (based on [11]).

quantities employed a bounded upwind differencing scheme of first-order accuracy. Diffusion terms were discretised using a corrected scheme for surface-normal gradients with a limiting coefficient of 0.5. Linear interpolation was used between cell centres and face centres.

The system of equations that resulted upon discretisation was solved using the iterative solver settings listed in Table 1. Pressure-velocity coupling was achieved using the semi-implicit method for pressure-linked equations (SIMPLE) algorithm. During each iteration, an inner-loop of the pressure equation was performed for non-orthogonal correction.

Solutions were deemed converged when the air mass flow rates through the fan and heat exchangers, heat transfer rates, and fan power consumptions stabilised. In the case of the windless computations, stabilised means that the final computed values were within 0.1% of the average of the last thousand computed values. For the simulations with wind, this tolerance increased to 0.5%. To be conservative, windless simulation results were rounded to the nearest 0.5%, and results reported for simulations under windy conditions were rounded to the nearest 1%.

The scaled residuals of the iterative solution procedures reduced to values in the order of 10^{-5} for the simulations without wind. In the cases of wind speeds of 3 and 6 m/s, the scaled residuals reached values in the order of 10^{-4}. For the highest wind speed of 9 m/s, however, looser convergence levels of only 10^{-3} were achievable. At such a high wind speed, the degree of flow separation downstream of the sharp corners of the ACC is greater, which results in higher residuals.

Sensitivity studies were performed for the models presented in the following subsections. Mesh densities were increased up to a point whereafter the fan and heat exchanger characteristics no longer changed upon refinement. The sensitivity to boundary distances was also investigated to ensure that the boundaries were far enough not to affect key results. The results presented in the remainder of this study are therefore deemed mesh and boundary-distance independent.

2.2. Axial flow fan model

The axial flow fans were modelled using the actuator disc model (ADM) of Thiart and Von Backström [11]. For each fan to be modelled,

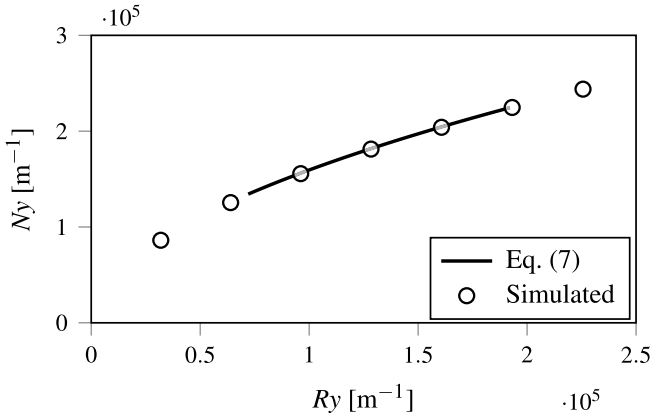

(a) Characteristic heat transfer parameter

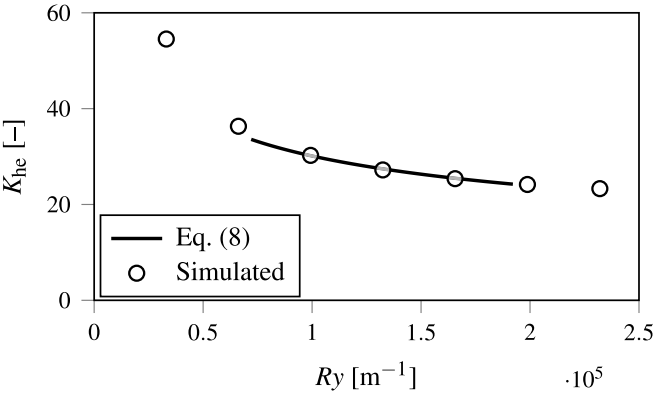

(b) Isothermal pressure loss coefficient

Fig. 2. Comparison between numerical solutions and empirical relations for the characteristic heat transfer parameter and isothermal pressure loss coefficient of the heat exchanger as a function of the characteristic flow parameter.

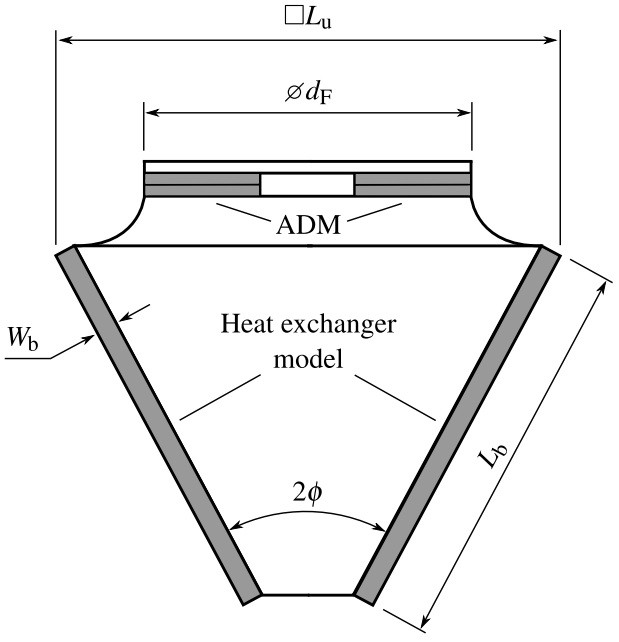

Fig. 3. Fan-unit schematic.

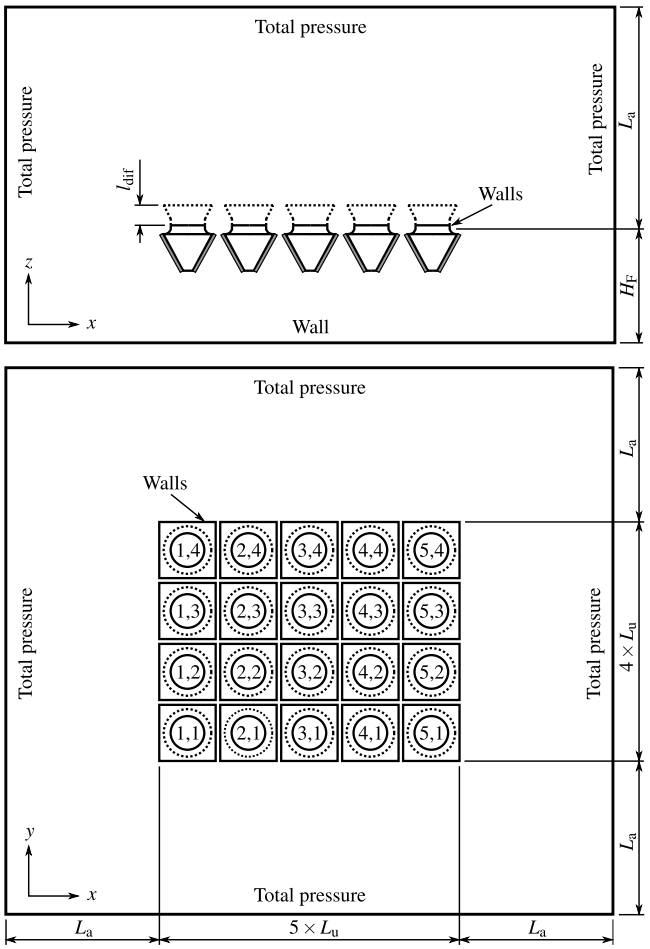

Fig. 4. Computational domain and boundary conditions for the 20-fan ACC.

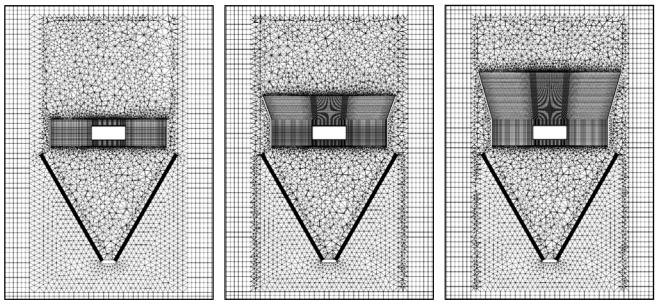

(a) Fan only (b) $l_{dif} = 0.2d_F$ (c) $l_{dif} = 0.4d_F$

Fig. 5. Meshes of the different fan-unit discharge configurations.

the ADM requires three identical axially aligned discs that are each one computational cell thick. The upstream and downstream discs are required to obtain the velocity vectors at the inlet and outlet of the fan, respectively. From these, the mean relative velocity vector, u_R, and relative flow angle, β, are calculated (see Fig. 1).

The fan blade forces are introduced into the momentum equations on a per volume basis. The axial component of the force is given by

$$\frac{\delta F_x}{\delta V} = \frac{1}{2}|u_R|^2 \frac{\sigma}{t}\left(C_L \cos\beta - C_D \sin\beta\right) \tag{1}$$

and the tangential component by

$$\frac{\delta F_\theta}{\delta V} = \frac{1}{2}|u_R|^2 \frac{\sigma}{t}\left(C_L \sin\beta + C_D \cos\beta\right) \tag{2}$$

Table 2
Fan-unit dimensions.

Dimension	Symbol	Value [m]
Fan-unit width and breadth	L_u	8.750
Fan diameter	d_F	7.315
Heat exchanger bundle length	L_b	7.750
Heat exchanger bundle width	W_b	0.208
V-frame apex angle	2ϕ	60°

Table 3
Single fan-unit validation results.

Operating point	Analytical	Numerical	Unit
Air volume flow rate	334.62	335.11	m^3/s
Fan power consumption	59.05	54.50	kW
Heat transfer rate	9.17	9.01	MW

Table 4
ACC domain dimensions.

Dimension	Symbol	Value [m]
Fan-unit width and breadth	L_u	8.75
Fan height	H_F	25
Atmospheric boundary distances	L_a	122.5
Diffuser length	l_{dif}	0.146 or 2.926

Table 5
ACC performance at $u_{ref} = 0\,m/s$ with different fan discharge configurations.

Performance metric	Fan only	$l_{dif} = 0.2d_F$ diffuser	$l_{dif} = 0.4d_F$ diffuser
Mean volumetric effectiveness	1.000	1.025	1.025
Mean thermal effectiveness	0.990	1.015	1.015

In Eqs. (1) and (2), $\sigma = n_{Fb}c/(2\pi r)$ is the solidity ratio of the fan (where n_{Fb} is the number of fan blades, c is the chord length at a given radial station, and r is the radius). The axial thickness of the actuator disc is denoted by t. Wilkinson [12, p. 43] obtained the lift and drag characteristics, C_L and C_D, of the M-fan blades using XFOIL [13]. The aerofoil thickness, camber, and chord-based Reynolds number were taken into account.

Bekker et al. [6] validated the M-fan model against the experimental measurements and simulated results of Wilkinson et al. [14]. They [6] found that the model accurately predicted the performance characteristics of the fan as well as the velocity profiles at the fan exit.

2.3. Heat exchanger model

The heat exchangers were modelled akin to the approach outlined by Engelbrecht et al. [15]. That is, the heat transfer rate from the process fluid to the air was modelled using the ϵ-NTU (effectiveness number of transfer units) method. The pressure drop and flow conditioning due to the heat exchangers were modelled using the Darcy-Forchheimer porosity model.

The heat transfer rate is calculated as [8]

$$\dot{Q} = \epsilon \dot{m}_a c_{p_{a,m}} \left(T_s - T_{a,i}\right) \tag{3}$$

where $\dot{m}_a$ is the air mass flow rate, and $c_{p_{a,m}}$ is the specific heat of air at the mean temperature across the heat exchanger, i.e. $T_{a,m} = \left(T_{a,i} + T_{a,o}\right)/2$. The steam temperature is denoted by T_s. The air temperatures entering and exiting the heat exchanger are denoted by $T_{a,i}$ and $T_{a,o}$, respectively. For a condensation process, the heat exchanger's effectiveness is given by [8]

$$\epsilon = 1 - \exp\left[-UA/\left(\dot{m}_a c_{p_{a,m}}\right)\right] \tag{4}$$

where the overall conductance of the heat exchanger can be approximated as [15]

$$UA \approx h_{a,m} A_{fr} = k_{a,m}\, Pr_{a,m}^{1/3}\, N\, y\, A_{fr} \tag{5}$$

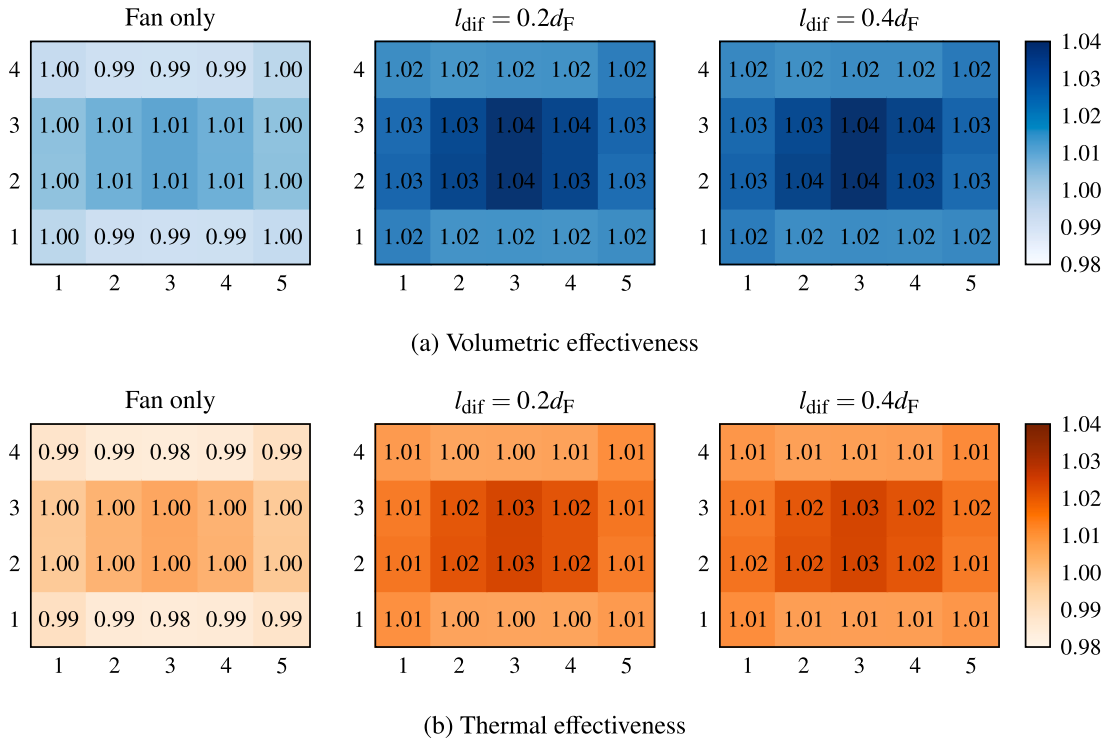

Fig. 6. ACC volumetric and thermal effectiveness under windless operating conditions.

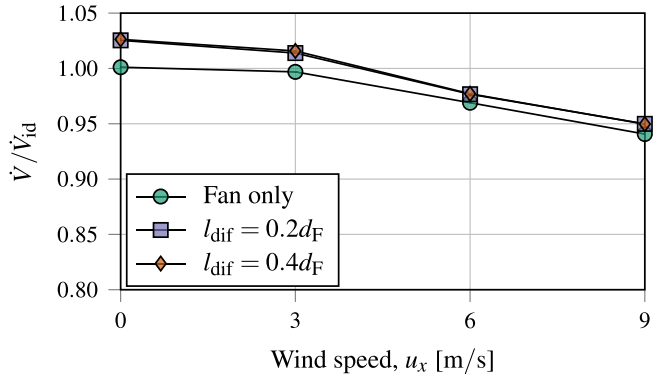

(a) Mean volumetric effectiveness

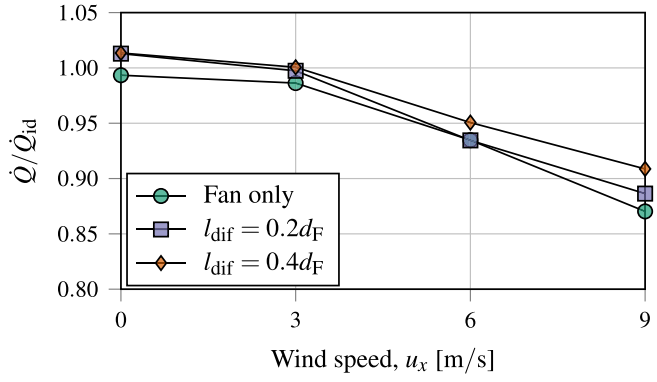

(b) Mean thermal effectiveness

Fig. 7. Effects of 3, 6 and 9 m/s winds in the x-direction on the ACCs' effectiveness.

In Eq. (5), $h_{a,m}$ is the mean air-side heat transfer coefficient, $k_{a,m}$ is the thermal conductivity of air evaluated at the mean temperature across the heat exchanger, and $Pr_{a,m}$ is the Prandtl number of air at this same temperature. A_{fr} is the frontal area of the heat exchanger, and Ny is the characteristic heat transfer parameter.

The pressure drop due to heat exchangers was modelled using the Darcy-Forchheimer porosity model. This model acts as a sink term in the momentum equation, taking the form of a pressure drop per unit length. In the direction normal to the plane of the heat exchanger, the pressure drop gradient is given by [9]

$$\frac{dp}{dn} \approx \frac{\Delta p_{he}}{W_{he}} = \mu_{a,i} k_D u_{he} + \rho_{a,i} k_F u_{he}^2/2 \tag{6}$$

where Δp_{he} is the pressure drop across the heat exchanger of width W_{he} at a mean velocity of u_{he}. The Darcy-Forchheimer coefficients are represented by k_D and k_F. Furthermore, $\mu_{a,i}$ and $\rho_{a,i}$ are the dynamic viscosity and density of air at the inlet temperature of the heat exchanger.

Kröger [8] states that if the loss coefficient of a heat exchanger is high, the flow will exit the heat exchanger perpendicularly. The Darcy-Forchheimer porosity model is capable of accounting for this flow conditioning: By specifying large k_D and k_F coefficients in the directions that are in-plane with the heat exchanger, the flow will pass through the heat exchanger in the desired perpendicular direction.

Heat exchanger bundles consisting of four rows of extruded bimetallic finned tubes were selected for the current study. Kröger [8] provides the heat transfer rate and pressure drop characteristics for this particular bundle. The empirical relation given for the characteristic heat transfer parameter is

$$Ny = 383.62\, Ry^{0.52} \tag{7}$$

and the relation given for the isothermal pressure loss coefficient is

$$K_{he} = \frac{\Delta p_{he}}{\rho_{a,m} |u_{he}|^2/2} = 1383.95\, Ry^{-0.33} \tag{8}$$

where $Ry = \dot{m}_a/(\mu_{a,i} A_{fr})$ is the characteristic flow parameter.

The heat exchanger model was validated by comparing simulated results to the empirical relations given by Eqs. (7) and (8). Heat

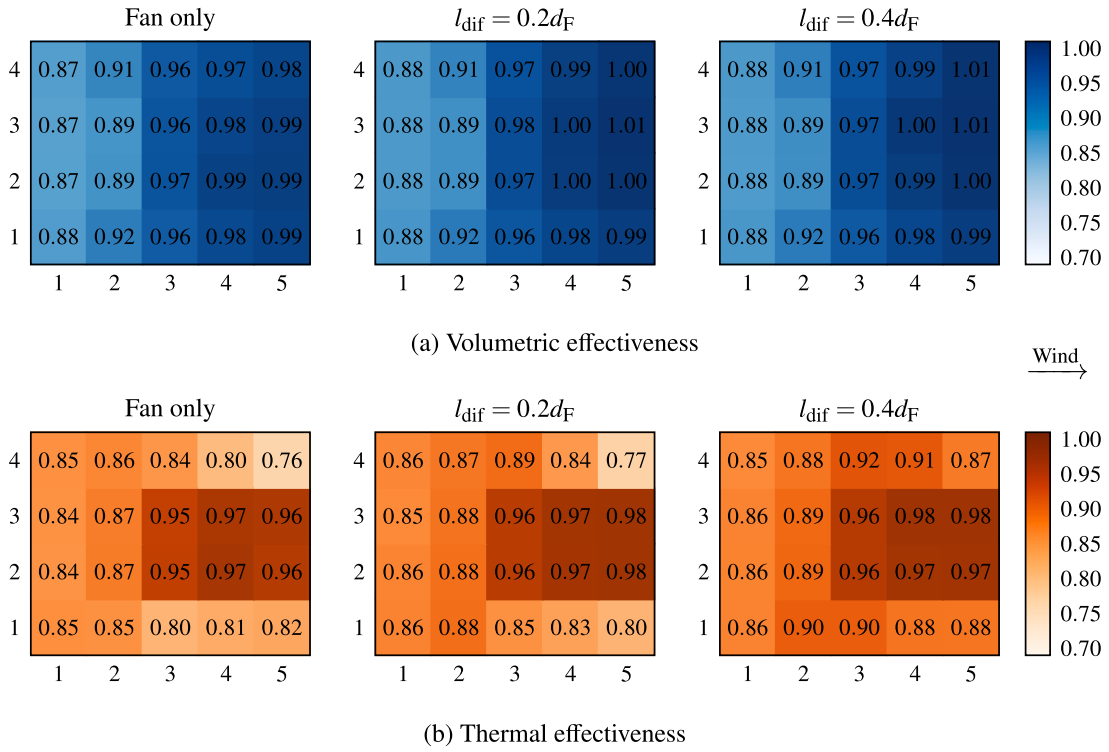

Fig. 8. ACC volumetric and thermal effectiveness at $u_x = 9\,\mathrm{m/s}$.

transfer rates and pressure drops were simulated at a range of air mass flow rates to obtain the characteristic curves presented in Fig. 2. The simulated results and empirical relations based on experimental measurements agree closely, validating the heat exchanger model.

2.4. Single-unit ACC model

Similar to Louw et al. [9], the induced draught ACC model was formed by combining the fan and heat exchanger models in a V-frame configuration. Fig. 3 depicts a schematic of a single fan unit, and its dimensions are listed in Table 2.

The ACC model was validated by comparing the simulated operating point of a free-standing fan unit to the solution of the theoretical draught equation for an induced draught ACC, given by Kröger [8]. The results are presented in Table 3. Note that the computational setup used for these simulations was similar to the setup outlined in the following section.

The operating air volume flow rates in Table 3 agree closely, i.e. within 0.5%. The numerical heat transfer rate is 1.5% lower than predicted by the draught equation. A discrepancy is expected, as the draught equation assumes uniform flow through the heat exchangers, whereas non-uniformity is present inside the plenum chamber of a V-frame fan unit [15]. Finally, the simulated fan power consumption is 7.5% lower than the analytical prediction. The fan performance characteristics of Wilkinson et al. [5] were used for the solution of the draught equation. They obtained these characteristics using a periodic three-dimensional fan model with no tip clearance. This model was found to produce higher fan power characteristics than the ADM. Since the ACC model employed the ADM, this 7.5% difference reinforces Wilkinson et al.'s [5] finding.

The agreement between the numerical and analytical solutions is deemed acceptable. The ACC model is therefore considered validated.

2.5. Multi-unit ACC model

An induced draught ACC model was created by copying and translating the single fan units of the previous section into a five-by-four array of fan units. This section outlines the computational setup that was used to simulate this 20-fan ACC.

2.5.1. Computational domain

The five-by-four ACC was located inside an atmospheric domain, as illustrated in Fig. 4. The dimensions of the computational domain are listed in Table 4.

2.5.2. Computational mesh

The computational domain was discretised following the same approach as Louw et al. [9]. That is, the mesh was constructed in a modular fashion, meshing separate sub-geometries and merging them to form the final mesh. The resulting meshes comprised of hexahedral, tetrahedral, and prismatic cells.

Fig. 5 illustrates the meshes used for the different fan discharge configurations investigated in this study. These fan units were copied, translated, and stitched together into a 20-fan ACC. An atmospheric region was then added around the fan units. The atmospheric sub-mesh consisted of hexahedra that were refined towards the ACC.

The mesh for the ACC devoid of diffusers consisted of 34.75 million cells. The meshes for the $l_{dif} = 0.2d_F$ and $l_{dif} = 0.4d_F$ diffuser ACCs comprised of 42.51 and 49.05 million cells, respectively. On average, the number of faces per cell in these meshes ranged from 5.0 to 5.2. The mean non-orthogonality of the meshes ranged from 13.3° to 14.2°, and the maximum cell skewness was 1.7.

2.5.3. Boundary conditions

A total pressure condition was applied to the atmospheric boundaries (top and sides) of the computational domain so that

$$p_{tot} = p_{ref} - \rho g z \tag{9}$$

where $p_{ref} = 101\,325\,\mathrm{Pa}$ at ground level, $\rho = p_{ref}/(RT)$, and z is the vertical distance measured from the ground. R is the gas constant, T is temperature, and g denotes gravitational acceleration.

In the absence of wind, the velocity at the atmospheric boundaries depended on the flux in the boundary-normal direction under inflow

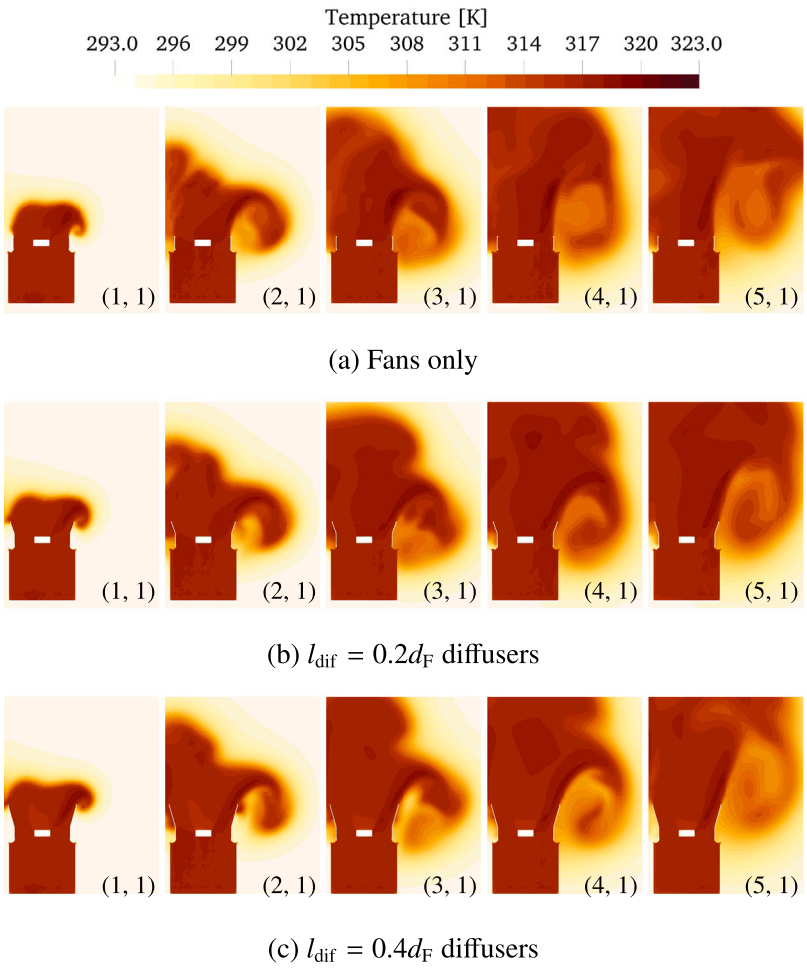

Fig. 9. Hot-plume recirculation along the side of the ACC for the different fan discharge configurations subjected to a wind speed of $u_x = 6\,\mathrm{m/s}$.

conditions. For outflow, it was treated as a zero-gradient condition. The temperature could vary at the boundaries, but for inflow, it was constrained to a fixed value of $T_{atm} = 20\,^{\circ}\mathrm{C}$. The k-ω turbulence variables were treated similar to temperature at these atmospheric boundaries. For flow entering the domain, a value of 0.1 was assigned to both k and ω.

For the simulation of wind, the atmospheric boundary layer profiles of Richards and Norris [16] were applied at the atmospheric inlet boundary, viz.

$$u = \frac{u_*}{\kappa}\ln\left(\frac{z+z_0}{z_0}\right) \tag{10}$$

$$k = \frac{u_*^2}{\sqrt{C_\mu}} \tag{11}$$

$$\omega = \frac{u_*}{\kappa z\sqrt{\beta^*}} \tag{12}$$

where u_* is the friction velocity, $\kappa = 0.41$ is the Von Kármán constant, and $C_\mu = \beta^* = 0.09$ for the k-ω turbulence model. In addition, z_0 is the surface roughness height and, akin to Louw et al. [9], was selected to be $z_0 = 0.1\,\mathrm{m}$. Richards and Hoxey [17] define the friction velocity as

$$u_* = u_{ref}\kappa \Big/ \ln\left(\frac{z_{ref}+z_0}{z_0}\right) \tag{13}$$

where u_{ref} is a reference velocity specified at a reference height of z_{ref}. The height of the ACC fans above ground level, i.e. $H_F = 25\,\mathrm{m}$, was selected as the reference height.

In the case of wind, symmetry conditions were applied to the atmospheric boundaries parallel to the wind direction (excluding the top boundary) to aid numerical stability. The size of the atmospheric region around the ACC was large enough to ensure a blockage ratio smaller than 3%, as advised by Tominaga et al. [18].

The ground and ACC walls were modelled as no-slip surfaces, utilising standard k-ω wall functions. However, the fan casing and diffuser walls did not have wall functions applied to them. Instead, multiple cell layers were added to these walls so that $y^+ \sim 1$. The turbulence variables were then set to $k = 0$ and $\omega = 6\nu/\left(\beta_1 y^2\right)$ [19].

3. ACC performance analysis

The performance of the five-by-four induced draught ACC is evaluated in this section. The ACC was first tested without any fan discharge appendages and then with the two different exhaust diffusers of Bekker et al. [6]. Initially, the performance was evaluated under windless conditions. Thereafter, it was analysed under the influence of three wind speeds: 3, 6 and 9 m/s in both the x- and y-directions.

3.1. Performance metrics

The volumetric effectiveness of an individual fan unit, $\dot{V}/\dot{V}_{id}$, is the ratio of the actual airflow rate through the fan unit to the airflow rate through that same free-standing unit operating under ideal conditions, i.e. without wind or flow obstructions. The ideal airflow rate is taken from the free-standing unit results contained in Table 3, i.e. $\dot{V}_{id} = 335.11\,\mathrm{m^3/s}$.

The thermal effectiveness of an individual fan unit, $\dot{Q}/\dot{Q}_{id}$, is the ratio of the actual rate of heat rejected by the heat exchangers in a

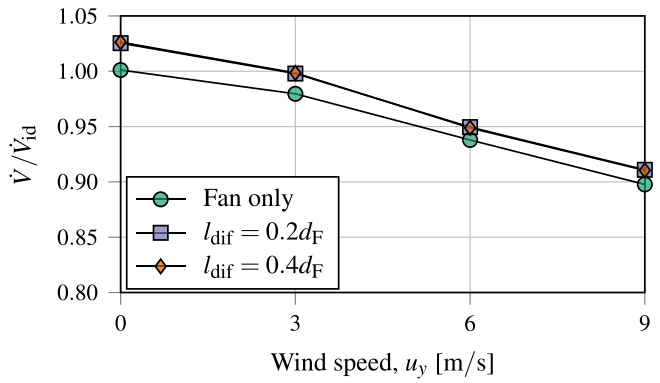

(a) Mean volumetric effectiveness

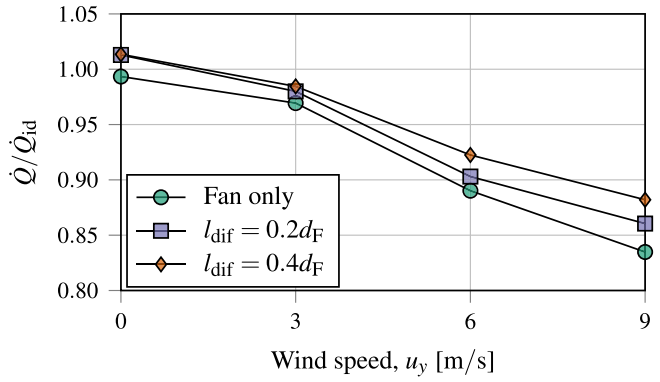

(b) Mean thermal effectiveness

Fig. 10. Effects of 3, 6 and 9 m/s winds in the *y*-direction on the ACCs' effectiveness.

fan unit to the ideal rate of heat rejected by that same free-standing unit under ideal conditions. From Table 3, the ideal heat transfer rate is taken as $\dot{Q}_{id} = 9.01$ MW.

Mean effectiveness values for the ACC were obtained by taking the arithmetic mean of the volumetric or thermal effectiveness values of the individual fan units within the ACC.

3.2. Windless operating conditions

The performance of the ACC without discharge diffusers is compared to the performance of the ACC after the $l_{dif} = 0.2d_F$ and $l_{dif} = 0.4d_F$ conical diffusers were attached to the fan outlets. These simulations were performed under windless conditions, i.e. $u_{ref} = 0$ m/s. Table 5 illustrates that both diffusers increased the ACC's mean volumetric effectiveness by 0.025 (or 2.5%) and its mean thermal effectiveness by 2.0%.

The volumetric and thermal effectiveness distributions of the ACCs are displayed in Fig. 6. Similar to the behaviour observed in forced draught ACCs [20], the periphery fan units yield lower effectiveness values than the inner units. Flow separation along the periphery of the ACC lowers the effectiveness of those units.

3.3. Windy operating conditions

The ACC benefited from the use of discharge diffusers under windless conditions. However, the $l_{dif} = 0.2d_F$ diffusers reduce the ACC's average discharge velocity from 8.0 to 6.2 m/s (i.e. a 22% reduction), and the $l_{dif} = 0.4d_F$ diffusers reduce it to 5.4 m/s (i.e. a 32% reduction). These lower discharge velocities could render the system more susceptible to hot-plume recirculation under windy conditions.

Therefore, the effects of wind on the performance of the ACCs are investigated in this section. Wind speeds of 3, 6 and 9 m/s at a reference height of $z_{ref} = H_F = 25$ m were applied in both the *x*- and *y*-directions. For each wind speed and direction, all three fan discharge configurations were investigated. The performance results for these 18 cases follow.

3.3.1. Wind in *x*-direction

Wind in the *x*-direction is along the longitudinal axis (or long axis) of the ACC, as indicated in Fig. 4. The mean volumetric and thermal effectivenesses of the different ACC configurations are plotted as a function of wind speed in Fig. 7. The effectiveness distributions at a wind speed of $u_x = 9$ m/s are displayed in Fig. 8. It can be seen that, even though the diffusers reduced the discharge velocities, the ACC still benefited from the use of diffusers under windy conditions.

The mean volumetric effectiveness of the diffuserless ACC declined from 1.000 under windless conditions by 3% at 6 m/s and by 6% at 9 m/s. At 3 m/s the decline in effectiveness was negligible. Fig. 7 illustrates that the improvements in mean volumetric effectiveness resulting from both diffusers were similar. At the tested wind speeds, the improvements ranged from 1–2%. Note that the ACC's volumetric effectiveness benefited ~1% less from the use of diffusers at the higher wind speeds than at $u_x = 3$ m/s. It was found that the velocity profiles at the fan inlets became distorted and asymmetric at higher wind speeds, especially in the wind-facing periphery units.

The diffusers were designed assuming axisymmetric inlet flow conditions [4,6]. Johnston [21] found that diffuser performance suffers due to inlet non-uniformity and asymmetry, especially in wide-angled diffusers. Sovran and Klomp [22] added that diffusers tend to amplify incoming non-uniformities. The non-uniformity and asymmetry at the diffuser inlets caused by wind therefore adversely affect the diffusers' performance. As a result, the fan performance gains from the diffusers diminish at higher wind speeds.

The mean thermal effectiveness of the ACC without diffusers decreased from 0.99 under windless conditions by 1% at 3 m/s, by 6% at 6 m/s, and by 12% at 9 m/s. Fig. 7 illustrates that the $l_{dif} = 0.4d_F$ diffuser improved the mean thermal effectiveness of the ACC more than the $l_{dif} = 0.2d_F$ diffuser did, especially at higher wind speeds. At $u_x = 3$ m/s, both diffusers increased the mean thermal effectiveness by ~1%. But at 6 and 9 m/s, the longer diffuser improved the mean thermal effectiveness by 2% and 4%, respectively, whereas the shorter diffuser increased it by approximately zero and 2% (i.e. 2% lower), respectively.

The mean volumetric effectiveness results obtained with the two different diffusers are similar, but the mean thermal effectiveness results differ. When the thermal effectiveness declines more due to wind than the volumetric effectiveness, it is indicative of hot-plume recirculation. This phenomenon occurs when heated air exiting the ACC fans circulates back to the heat exchangers, raising inlet air temperatures. In such a case, the heat exchangers' capability of rejecting heat declines (see Eq. (3)). Due to vortices that form along the sides of the ACC under windy conditions, the fan units along the periphery of the ACC that are parallel to the wind direction are affected most by hot-plume recirculation (see Fig. 9). These vortices are seen to grow in size along the length of the ACC, which is why the fan units farther downwind suffer most from hot-plume recirculation (see Fig. 8).

The ACC featuring the longer diffuser suffered less from hot-plume recirculation than the ACC with the shorter diffuser. This is evident from Fig. 8: At $u_x = 9$ m/s, the mean thermal effectiveness of the periphery units parallel with the wind is 0.88 in the $l_{dif} = 0.4d_F$ diffuser ACC. In the $l_{dif} = 0.2d_F$ diffuser ACC, it is 0.84 (i.e. 4% lower). Yet the mean volumetric effectiveness of those periphery units in both the shorter and longer diffuser ACCs is 0.95.

Even though the longer diffusers reduced the average discharge velocity of the ACC more than the shorter diffusers, the ACC with the longer diffusers suffered less from hot-plume recirculation. An explanation for this is that the $l_{dif} = 0.4d_F$ diffuser is simply longer.

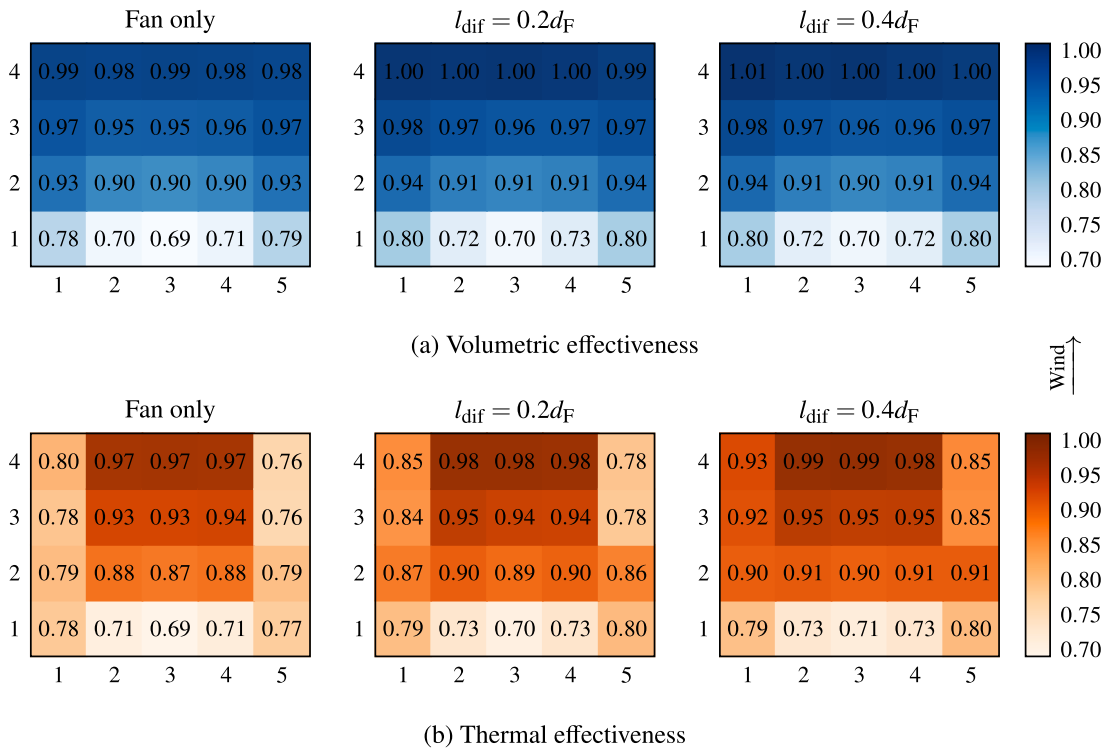

Fig. 11. ACC volumetric and thermal effectiveness at $u_y = 9\,\text{m/s}$.

The hot air thus discharges farther away from the heat exchangers, inhibiting the effluent air from circulating back to the heat-exchanger inlets. The divergence angle of the longer diffuser is also less acute than the shorter diffuser's (i.e. 32° versus 40°). The former therefore directs the flow more vertically upward than the latter does.

3.3.2. *Wind in y-direction*

Wind in the y-direction is parallel to the heat exchangers and along the shorter axis of the ACC, as indicated in Fig. 4. In Fig. 10, the mean volumetric and thermal effectivenesses are plotted as a function of wind speed for the different ACC discharge configurations. Fig. 11 depicts the effectiveness distributions at a wind speed of $u_y = 9\,\text{m/s}$. Again, the ACC benefited from the use of diffusers over the considered range of wind speeds.

The mean volumetric effectiveness of the ACC devoid of diffusers deteriorated from 1.00 under windless conditions by 2% at 3 m/s, by 6% at 6 m/s, and by 10% at 9 m/s. As before, the improvements in mean volumetric effectiveness resulting from the two different diffusers are essentially identical. At 3 to 9 m/s wind speeds, the diffusers increased the ACC's volumetric effectiveness by 1–2%. And again, the mean volumetric effectiveness benefited ~1% less from the use of diffusers at the higher wind speeds than at $u_y = 3\,\text{m/s}$. This slight decline in diffuser performance at higher wind speeds is also attributed to the flow distortion wind causes at the fan inlets.

The mean thermal effectiveness of the diffuserless ACC decreased from 0.99 under windless conditions by 2% at 3 m/s, by 10% at 6 m/s, and by 16% at 9 m/s. Fig. 10 illustrates that the improvements in mean thermal effectiveness obtained with the shorter diffuser were again inferior to those obtained with the longer diffuser at higher wind speeds. At 3 m/s, both diffusers increased the mean thermal effectiveness by 1–2%. However, at 6 and 9 m/s, the $l_{dif} = 0.4d_F$ diffusers produced 3 and 5% increases, respectively, whereas the $l_{dif} = 0.2d_F$ diffusers produced increases of only 1% and 3% (i.e. 2% lower), respectively.

Contrary to the expected effects of reduced discharge velocities, the diffusers aided in combating hot-plume recirculation. For the ACC without diffusers, the difference between the mean volumetric and thermal effectiveness of the periphery units parallel with the wind was 14% at $u_y = 9\,\text{m/s}$. For the ACC with $l_{dif} = 0.2d_F$ diffusers, this difference was 11%. And for the $l_{dif} = 0.4d_F$ diffuser ACC, the difference was 6%. The greater the difference between the thermal and volumetric effectiveness, the more hot-plume recirculation is contributing towards the decline in thermal effectiveness. The ACC utilising the longer diffuser, therefore, suffers significantly less from hot-plume recirculation (see Fig. 12). The reason for this is the same as before, i.e. that the longer diffuser shifts the discharge plane of the ACC farther away from the heat exchangers than the other discharge configurations.

3.3.3. *Comparison between x- and y-direction winds*

Comparing the mean effectivenesses of the ACCs in Figs. 7 and 10, it is evident that ACC performance deteriorates more due to wind in the y-direction as opposed to wind in the x-direction. Summarising from the diffuserless ACC results presented earlier, the mean volumetric effectiveness declines by 2–4% more for wind speeds of 3 to 9 m/s in the y-direction than in the x-direction. The reason for the lower volumetric performance in the case of y-direction winds is twofold.

Firstly, the greatest decline in fan performance is seen in the wind-facing periphery units (see Figs. 8 and 11). Since there are five wind-facing periphery units in the y-direction and only four in the x-direction, the ACC's performance is expected to be more sensitive to y-direction winds. Engelbrecht [23, p. 80] noted similar behaviour in a six-by-five forced draught ACC.

Secondly, the decline in fan performance in the upwind periphery units is more severe for wind in the y-direction (compare Figs. 8 and 11). To illustrate, a wind of $u_y = 9\,\text{m/s}$ decreases the mean volumetric effectiveness of the wind-facing periphery units by 26%, whereas a $u_x = 9\,\text{m/s}$ wind decreases it by only 13% (i.e. 13% less). That is because, owing to the V-frame geometry of the fan units, the degree of flow distortion at the wind-facing periphery units is greater for y-direction winds [9]. In the x-direction, wind aids in forcing air through the (slanted and permeable) wind-facing heat exchangers, but it also accelerates the air around the bottom vertices of the V-frames, causing flow separation. The separation starves the downwind heat

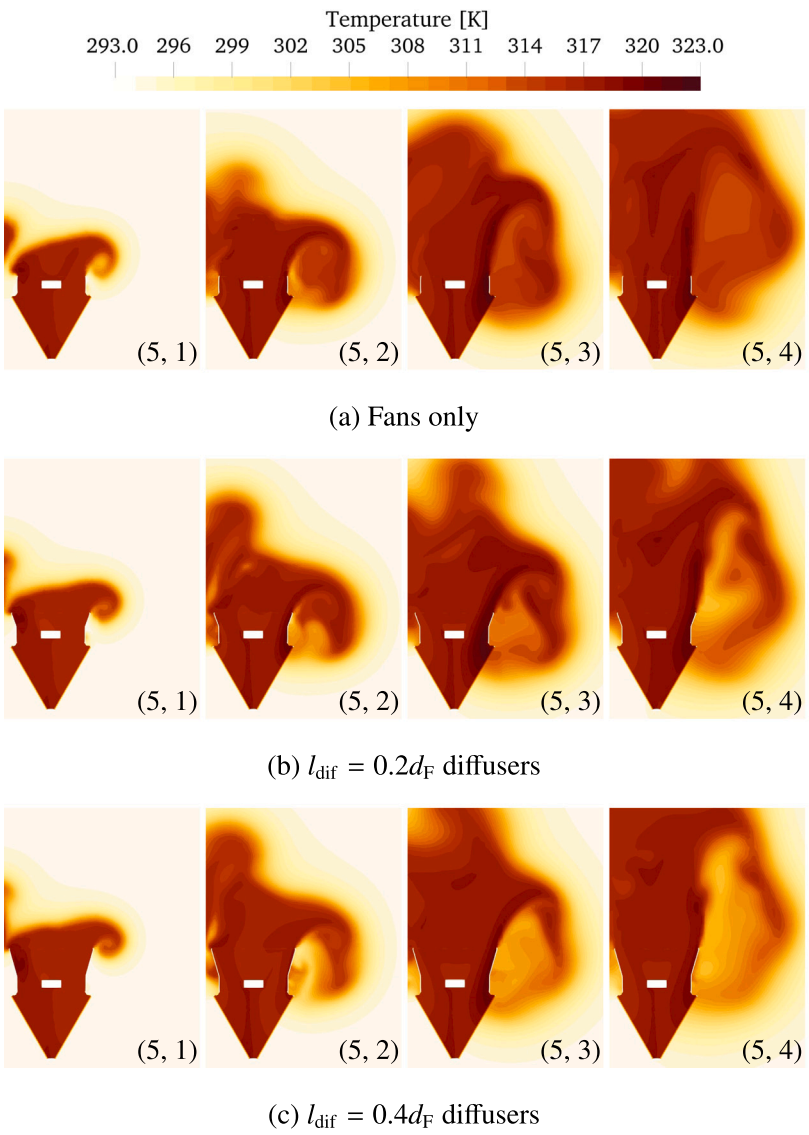

Fig. 12. Hot-plume recirculation along the side of the ACC for the different fan discharge configurations subjected to a wind speed of $u_y = 6\,\mathrm{m/s}$.

exchangers of air, lowering the effectiveness of those periphery units. Wind in the y-direction, on the other hand, strikes the (flat and solid) plenum chamber walls of the wind-facing periphery units. The air then accelerates around the corners of the plenum chambers, starving the heat exchangers of air on both sides of the units.

In terms of thermal performance, the ACC is also more sensitive to y-direction winds: For the ACC without diffusers, the mean thermal effectiveness decreases by 2–4% more due to wind speeds of 3 to 9 m/s in the y-direction than in the x-direction. The reason therefore is also twofold.

Firstly, since fan performance deteriorates more due to y-direction winds, the air mass flow rate through the heat exchangers also declines more under y-direction wind conditions. This reduces the heat transfer rate (see Eq. (3)).

Secondly, the difference between the volumetric and thermal effectiveness values for the periphery units that are parallel with the wind are generally greater for y-direction winds (compare Figs. 8 and 11). In other words, the ACC suffers more from hot-plume recirculation when the wind is from the y-direction. This can also be explained by the geometry of the V-frame fan units: For wind in the y-direction, the heat exchangers lie along the sides of the ACC and can easily draw in heated effluent air. For wind in the x-direction, however, the plenum chamber walls are along the sides of the ACC. These walls aid in blocking hot air from entering the heat exchangers.

Focusing on the effects of the diffusers, both diffusers produced similar mean volumetric effectiveness improvements whether the wind was from the x- or y-direction. The improvements in mean thermal effectiveness from the use of diffusers were, however, 1–2% greater at wind speeds of 6 and 9 m/s in the y-direction than in the x-direction.

The use of diffusers was found to reduce hot-plume recirculation, as diffusers shift the discharge plane of the ACC farther away from the heat exchangers. Hot-plume recirculation was found to reduce the ACC's thermal effectiveness more under y-direction wind conditions. Therefore, the addition of diffusers benefits the thermal effectiveness of the ACC more under y-direction wind conditions.

4. Conclusion

This paper investigated the potential gains in performance of an induced draught air-cooled condenser (ACC) resulting from pressure recovery. Performance was measured using the volumetric effectiveness, $\dot{V}/\dot{V}_{id}$, and the thermal effectiveness, $\dot{Q}/\dot{Q}_{id}$, of the entire ACC as well as the effectivenesses of the individual fan units within the ACC. The ACC's performance was evaluated under windless conditions and

under the influence of wind speeds of 3, 6 and 9 m/s in both the x- and y-directions. Two conical diffuser designs were tested as discharge configurations for the ACC: a shorter diffuser of length $l_{dif} = 0.2d_F$ with an included angle of $2\theta = 40°$, and a longer diffuser of length $l_{dif} = 0.4d_F$ and $2\theta = 32°$.

Under windless operating conditions, both diffusers increased the mean volumetric effectiveness of the ACC by 2.5% and the mean thermal effectiveness by 2.0%.

Under windy operating conditions, both diffusers increased the mean volumetric effectiveness of the ACC by 1–2% over the considered range of wind speeds. However, due to higher non-uniformity and asymmetry at the fan inlets, the benefits from the diffusers were ~1% lower at wind speeds of 6 and 9 m/s than at 3 m/s.

Although the diffusers reduced the average discharge velocity of the ACC by 22–32%, they were found to benefit the thermal effectiveness of the ACC under windy conditions. Attaching diffusers to the fan outlets shifts the discharge plane of the ACC farther away from the heat exchangers, which inhibits hot-plume recirculation. For this reason, the longer diffuser produced higher thermal effectiveness improvements than the shorter diffuser: The $l_{dif} = 0.2d_F$ diffuser increased the mean thermal effectiveness of the ACC by 0–2%, whereas the $l_{dif} = 0.4d_F$ diffuser increased it by 1–5%.

Wind from the y-direction had a more detrimental effect on the ACC's performance than x-direction winds. This was attributed to the fact that there are more wind-facing periphery units in the case of wind in the y-direction. In addition, because of the shape of the V-frame fan units, the degree of flow distortion at the upwind periphery units was greater for y-direction winds. Even so, the gains in fan performance resulting from the added diffusers were similar under x- and y-direction wind conditions. Also as a result of the fan units' V-frame geometry, the ACC was more susceptible to hot-plume recirculation when subjected to y-direction winds. Since the tested diffusers were found to reduce hot-plume recirculation, the thermal effectiveness of the ACC benefited more from the use of diffusers under y-direction wind conditions.

The percentage performance improvements quoted in this paper resulting from the added discharge diffusers are relatively small. Nevertheless, given the size of ACCs in large power plants and frequency at which they operate, even small percentage performance improvements yield significant energy and running-cost savings. The findings in this paper therefore advocate the use of well-designed discharge diffusers in an induced draught ACC.

Although the overall performance of the ACC fitted with the longer $l_{dif} = 0.4d_F$ conical diffuser was better, the shorter $l_{dif} = 0.2d_F$ diffuser might be more suited for practical application. The latter has various practical advantages over the longer diffuser, such as lower costs associated with manufacturing, transportation and installation. A combination of these diffusers could also be considered: Both diffusers increased the airflow rate through the ACC similarly, but the longer diffuser resulted in less hot-plume recirculation. Therefore, the longer diffuser could be used for the fan units along the periphery of the ACC to aid in combating hot-plume recirculation, and the shorter diffuser could be used for the inner units to save costs.

Declaration of competing interest

The authors declare that they have no known competing financial interests or personal relationships that could have appeared to influence the work reported in this paper.

Acknowledgements

The authors acknowledge the Centre for High Performance Computing (CHPC), South Africa, for providing computational resources for this research.

The authors acknowledge Daniel Louw for sharing and assisting with the implementation of the ACC numerical models.

Funding

This work was supported by the Centre for Renewable and Sustainable Energy Studies (CRSES) [grant number DST/CON0230/2017]; the Solar Thermal Energy Research Group (STERG), South Africa; and the Department of Mechanical and Mechatronic Engineering of Stellenbosch University, South Africa.

References

[1] R.A. Wallis, Axial Flow Fans and Ducts, John Wiley & Sons, Inc., 1983.
[2] B. Eck, Fans: Design and Operation of Centrifugal, Axial-Flow and Cross-Flow Fans, Pargamon Press Ltd., 1973.
[3] J. Walter, S. Caglar, M. Gabi, Investigation of the maximum static efficiency of axial fans, in: International Conference of Fan Noise, Aerodynamics, Applications and Systems, Darmstadt, Germany, 11–18 April, 2018.
[4] G.M. Bekker, C.J. Meyer, S.J. Van der Spuy, Numerical investigation of pressure recovery for an induced draught fan arrangement, R & D J. 36 (2020) 19–28, http://dx.doi.org/10.17159/2309-8988/2020/v36a3.
[5] M.B. Wilkinson, S.J. Van der Spuy, T.W. Von Backström, The design of a large diameter axial flow fan for air-cooled heat exchanger applications, in: ASME Turbo Expo 2017: Turbomachinery Technical Conference and Exposition, Charlotte, North Carolina, USA, 26–30 June, Vol. 1, ASME, 2017, http://dx.doi.org/10.1115/GT2017-63331.
[6] G.M. Bekker, C.J. Meyer, S.J. Van der Spuy, Performance enhancement of an induced draught axial flow fan through pressure recovery, R & D J. 37 (2021) 35–44, http://dx.doi.org/10.17159/2309-8988/2021/v37a5.
[7] ISO 5801, Industrial Fans: Performance Testing Using Standardized Airways, International Organization for Standardization, 2007.
[8] D.G. Kröger, Air-Cooled Heat Exchangers and Cooling Towers: Thermal-Flow Performance Evaluation and Design, Department of Mechanical Engineering, Stellenbosch University, South Africa, 1998.
[9] D.L. Louw, C.J. Meyer, S.J. Van der Spuy, Numerical investigation of an induced draft air-cooled condenser under crosswind conditions, in: ASME 2021 Summer Heat Transfer Conference, Virtual, Online, 16–18 June, ASME, 2021, http://dx.doi.org/10.1115/HT2021-62355.
[10] D.C. Wilcox, Turbulence Modeling for CFD, second ed., DCW Industries, 1998.
[11] G.D. Thiart, T.W. Von Backström, Numerical simulation of the flow field near an axial flow fan operating under distorted inflow conditions, J. Wind Eng. Ind. Aerodyn. 45 (2) (1993) 189–214, http://dx.doi.org/10.1016/0167-6105(93)90270-X.
[12] M.B. Wilkinson, The Design of an Axial Flow Fan for Air-Cooled Heat Exchanger Applications (Master's thesis), Department of Mechanical and Mechatronic Engineering, Stellenbosch University, 2017, URL http://hdl.handle.net/10019.1/102840.
[13] M. Drela, XFOIL: An analysis and design system for low Reynolds number airfoils, in: T.J. Mueller (Ed.), Low Reynolds Number Aerodynamics, in: Lecture Notes in Engineering, vol. 54, Springer, Berlin, Heidelberg, 1989, pp. 1–12, http://dx.doi.org/10.1007/978-3-642-84010-4_1.
[14] M.B. Wilkinson, S.J. Van der Spuy, T.W. Von Backström, Performance testing of an axial flow fan designed for air-cooled heat exchanger applications, in: ASME Turbo Expo 2018: Turbomachinery Technical Conference and Exposition, Oslo, Norway, 11–15 June, Vol. 1, ASME, 2018, http://dx.doi.org/10.1115/GT2018-75964.
[15] R.A. Engelbrecht, C.J. Meyer, S.J. Van der Spuy, Modeling strategy for the analysis of forced draft air-cooled condensers using rotational fan models, J. Therm. Sci. Eng. Appl. 11 (5) (2019) 051011, http://dx.doi.org/10.1115/1.4042590.
[16] P.J. Richards, S.E. Norris, Appropriate boundary conditions for computational wind engineering models revisited, J. Wind Eng. Ind. Aerodyn. 99 (2011) 257–266, http://dx.doi.org/10.1016/j.jweia.2010.12.008.
[17] P.J. Richards, R.P. Hoxey, Appropriate boundary conditions for computational wind engineering models using the k-ε turbulence model, J. Wind Eng. Ind. Aerodyn. 46–47 (1993) 145–153, http://dx.doi.org/10.1016/0167-6105(93)90124-7.
[18] Y. Tominaga, A. Mochida, R. Yoshie, H. Kataoka, T. Nozu, M. Yoshikawa, T. Shirasawa, AIJ guidelines for practical applications of CFD to pedestrian wind environment around buildings, J. Wind Eng. Ind. Aerodyn. 96 (10–11) (2008) 1749–1761, http://dx.doi.org/10.1016/j.jweia.2008.02.058.
[19] D.C. Wilcox, Reassessment of the scale-determining equation for advanced turbulence models, AIAA J. 26 (11) (1988) 1299–1310, http://dx.doi.org/10.2514/3.10041.

[20] C.A. Salta, D.G. Kröger, Effect of inlet flow distortions on fan performance in forced draught air-cooled heat exchangers, Heat Recov. Syst. CHP 15 (6) (1995) 555–561, http://dx.doi.org/10.1016/0890-4332(95)90065-9.

[21] I.H. Johnston, The Effect of Inlet Conditions on the Flow in Annular Diffusers, Tech. Rep. M. 167, National Gas Turbine Establishment, United Kingdom, 1953, URL https://apps.dtic.mil/sti/pdfs/AD0018166.pdf.

[22] G. Sovran, E.D. Klomp, Experimentally determined optimum geometries for rectilinear diffusers with rectangular, conical or annular cross-section, in: G. Sovran (Ed.), Fluid Mechanics of Internal Flow: Proceedings of the Symposium on the Fluid Mechanics of Internal Flow, General Motors Research Laboratories, Warren, Michigan, 1965, Elsevier, 1967, pp. 270–319.

[23] R.A. Engelbrecht, Numerical Investigation of Fan Performance in a Forced Draft Air-Cooled Condenser (Ph.D. thesis), Department of Mechanical and Mechatronic Engineering, Stellenbosch University, 2018, URL http://hdl.handle.net/10019.1/105082.